

Geophysical Research Letters[®]



RESEARCH LETTER

10.1029/2024GL109179

Key Points:

- Using a fuzzy categorization, five different El Niño Southern Oscillation (ENSO) types are identified in observations
- Extreme El Niño events emerge as a distinct category
- Strong La Niña and Extreme El Niño categories mainly contributed to the shift in decadal ENSO variance around 1970

Supporting Information:

Supporting Information may be found in the online version of this article.

Correspondence to:

J. Schlör,
jakob.schloer@uni-tuebingen.de

Citation:

Schlör, J., Strnad, F., Capotondi, A., & Goswami, B. (2024). Contribution of El Niño Southern Oscillation (ENSO) diversity to low-frequency changes in ENSO variance. *Geophysical Research Letters*, 51, e2024GL109179. <https://doi.org/10.1029/2024GL109179>

Received 12 MAR 2024

Accepted 9 JUL 2024





Author Contributions:

Conceptualization: Jakob Schlör, Antonietta Capotondi, Bedartha Goswami
Formal analysis: Jakob Schlör
Funding acquisition: Antonietta Capotondi, Bedartha Goswami
Investigation: Jakob Schlör
Methodology: Jakob Schlör, Felix Strnad
Project administration: Antonietta Capotondi, Bedartha Goswami
Software: Jakob Schlör, Felix Strnad
Supervision: Antonietta Capotondi, Bedartha Goswami
Validation: Jakob Schlör, Felix Strnad
Visualization: Jakob Schlör
Writing – original draft: Jakob Schlör
Writing – review & editing: Jakob Schlör, Felix Strnad, Antonietta Capotondi, Bedartha Goswami

© 2024. The Author(s).

This is an open access article under the terms of the [Creative Commons Attribution License](https://creativecommons.org/licenses/by/4.0/), which permits use, distribution and reproduction in any medium, provided the original work is properly cited.

Contribution of El Niño Southern Oscillation (ENSO) Diversity to Low-Frequency Changes in ENSO Variance

Jakob Schlör¹ , Felix Strnad¹ , Antonietta Capotondi^{2,3} , and Bedartha Goswami¹ 

¹Machine Learning in Climate Science, University of Tübingen, Tübingen, Germany, ²Cooperative Institute for Research in Environmental Sciences, University of Colorado, Boulder, CO, USA, ³NOAA Physical Sciences Laboratory, Boulder, CO, USA

Abstract El Niño Southern Oscillation (ENSO) diversity is characterized based on the longitudinal location of maximum sea surface temperature anomalies (SSTA) and amplitude in the tropical Pacific, as Central Pacific events are typically weaker than Eastern Pacific events. SSTA pattern and intensity undergo low-frequency modulations, affecting ENSO prediction skill and remote impacts, and resulting in low-frequency changes in ENSO variance. Yet, how different ENSO types contribute to these decadal variance changes remains unclear. Here, we decompose the low-frequency changes of ENSO variance into contributions from ENSO diversity categories. We propose a fuzzy clustering of monthly SSTA to allow for non-binary event category memberships, where each event can belong to different clusters. Our approach identifies two La Niña and three El Niño categories and shows that the major shift of ENSO variance in the mid-1970s was associated with an increasing likelihood of strong La Niña and extreme El Niño events.

Plain Language Summary The El Niño Southern Oscillation (ENSO) is a climate phenomenon that involves changes in ocean temperatures in the central and eastern tropical Pacific and greatly influences the weather around the globe. ENSO events are usually categorized based on where these temperature variations are the strongest and how intense they are. However, these categories are at times ambiguous and the way ENSO behaves can change over decades. Our study introduces a new way to estimate how different kinds of ENSO events contribute to its overall variation over time. We base our variability analysis on a fuzzy categorization of ENSO events, which results in three different kinds of El Niño events and two kinds of La Niña events. We find that the decadal changes in ENSO variance, including the decadal shift in the mid-1970s, were primarily associated with strong La Niña and extreme El Niño events.

1. Introduction

The El Niño-Southern Oscillation (ENSO), characterized by anomalous sea surface temperatures (SSTs) in the tropical Pacific, exhibits notable diversity in its amplitude, temporal evolution, and spatial pattern. The El Niño events of 1982–1983 and 1997–1998, for instance, recorded exceptionally high SST anomaly (SSTA) values in the eastern equatorial Pacific, whereas the El Niño of 2002–2003 was less extreme and exhibited the largest anomalies in the central equatorial Pacific (McPhaden, 2004). In order to describe these event-to-event differences, El Niño events have been generally categorized as Eastern Pacific (EP), and Central Pacific (CP) types (Capotondi et al., 2015). Eastern Pacific El Niño events typically have their peak SSTA in the EP, may exhibit stronger intensities, and a largely reduced zonal thermocline slope, resulting in the pronounced discharge of warm water from the equatorial thermocline. In contrast, CP events show peak SSTA in the CP and are comparatively weaker with smaller changes in zonal thermocline slope and warm water discharge (Capotondi, 2013; Kug et al., 2009).

These different types of ENSO events have substantially different downstream impacts on the global climate (e.g., Ashok et al., 2007; Beniche et al., 2024; Larkin & Harrison, 2005; Strnad et al., 2022). For example, extreme drought conditions were recorded in eastern Australia in 2002, while a minor impact on precipitation was detected during the extreme 1997 event (Wang & Hendon, 2007). Weaker and shorter-lived CP events are associated with warm conditions in the equatorial Atlantic during boreal winter, while stronger and persistent EP events lead to cold anomalies in that area, with different impacts on precipitation over northeastern Brazil (Kao & Yu, 2009; Rodrigues et al., 2011). Thus, a deeper understanding of ENSO diversity is critical to support predictions of ENSO impacts.

ENSO characteristics, including amplitude and spatial pattern, exhibit decadal variations, which are mediated by changes in the background state of the tropical Pacific (Capotondi et al., 2023). Notable decadal phase transitions were observed in the late 1970s (Miller et al., 1994) and around the year 2000 (McPhaden, 2012). Paleoclimate data also indicate an increase in ENSO amplitude over recent decades (Grothe et al., 2020), consistent with modeling results showing a significant increase in ENSO amplitude after 1960, which was attributed to anthropogenic forcing (Cai et al., 2023). Analysis of a large number of observationally-based data sets revealed that the longitudinal location of the maximum SST anomalies, as well as the intensity of both El Niño and La Niña events, undergo decadal fluctuations (Dieppois et al., 2021), which can, in turn, modulate ENSO predictions (Lou et al., 2023). However, event location and intensity were considered separately by Dieppois et al. (2021), so the contribution of different ENSO types to these decadal changes and long-term trends in ENSO variance remains unclear. Paleoclimate data (Lawman et al., 2022) indicate that extreme ENSO events may contribute to increases in ENSO variance. Similarly, climate models that capture relevant aspects of ENSO nonlinearities project an increase in ENSO variance that is linked to an increase in the frequency of extreme ENSO events (Cai et al., 2021). However, a more comprehensive understanding of these changes from an ENSO diversity perspective is still missing.

One main reason hindering the estimation of the contribution of different ENSO categories to its decadal modulation is that ENSO classifications often depend on the chosen definitions (Abdelkader Di Carlo et al., 2023; Capotondi, Wittenberg, et al., 2020; Pascolini-Campbell et al., 2015; J.-Y. Yu & Kim, 2013). The disagreement between different ENSO classification methods is likely due to the assumption that ENSO events can be classified into binary types, based on indices capturing the location of the highest SSTA in the Tropical Pacific (like the Niño3 and Niño4 regions), or using Empirical Orthogonal Functions (EOFs) (Ashok et al., 2007; Kao & Yu, 2009; Kug et al., 2009; Takahashi et al., 2011). However, ENSO events are continuously distributed in the space spanned by the two leading principal components (PCs) (Cai et al., 2018; Capotondi, Wittenberg, et al., 2020; Takahashi & Dewitte, 2016). Approaches that use a more continuous distribution of SSTAs to identify diversity show that events occur over multiple locations but with enhanced probabilities over the central and eastern tropical Pacific (Dieppois et al., 2021; Shin et al., 2021). In addition, both EP- and CP-type events appear to share common underlying dynamical processes, albeit with varying relevance depending on the longitude (Capotondi, 2013).

A notable example of an El Niño that eludes a binary classification is the 2015–2016 event. While its SSTA and several of its impacts were typical of extreme EP events (Santoso et al., 2017), this event was not associated with a significant impact on California precipitation and was not followed by a strong La Niña, as other events of this type (i.e., 1982–1983 and 1997–1998). Indeed, this event was considered a mixture of EP and CP types (Capotondi, Wittenberg, et al., 2020; Paek et al., 2017).

Here, we propose a new approach for characterizing ENSO diversity to better understand its relationship with decadal changes in ENSO variance. To that end, we develop a fuzzy clustering of the low-dimensional representation of monthly SSTA in the PC1-PC2 space to achieve a non-binary event categorization where individual events are assigned a probability of belonging to a given cluster. Such membership probabilities are then used to determine their relative contributions to the low-frequency ENSO variance.

2. Methodology and Data

2.1. Data

Our analysis is conducted on monthly SSTA in the tropical Pacific (130°E–70°W, 30°S–30°N) from eight reanalysis data sets merged together (Table S1 and Text S1 in Supporting Information S1). To ensure the same number of data points per month, we randomly select four data points per month from the eight data sets covering 1901–2022. While the dimensionality reduction encompasses all months, we select El Niño and La Niña winter months for the fuzzy clustering. Boreal winters (December–January–February (DJF)) are selected as El Niño (La Niña) when the average SSTA in the Niño3.4 region is larger than 0.5 K (smaller than −0.5 K).

2.2. Fuzzy Clustering

Clustering algorithms are typically based on a distance measure between data points which becomes ill-posed in high-dimensional spaces (Parsons et al., 2004). To mitigate this issue, we first reduce the dimensionality of the geospatial fields using EOF analysis before applying fuzzy clustering.

Our input data, $X = (x(t_1), \dots, x(t_N))$, which consists of tropical Pacific SSTA fields $x(t) \in \mathcal{R}^{N_{\text{lon}} \cdot N_{\text{lat}}}$, are projected onto the first two EOF patterns to obtain the two PCs $z(t) \in \mathcal{R}^2$, referred to as a latent vector. Besides EOFs, we also use a nonlinear dimensionality reduction method, specifically a convolutional autoencoder neural network (Text S2, Figure S1 in Supporting Information S1).

We apply the Gaussian Mixture Model (GMM), a probabilistic unsupervised clustering approach to identify different types of ENSO events. GMMs describe each cluster via a multivariate Gaussian distribution, accommodating overlapping probabilities. Mathematically, GMMs assume that the probability distribution of latent states, $p(z)$, comprises a mixture of Gaussians:

$$p(z) = \sum_{k=1}^K \pi_k \mathcal{N}(z | \mu_k, \Sigma_k), \quad (1)$$

with K representing the number of Gaussians, $\mathcal{N}(z | \mu_k, \Sigma_k)$, each characterized by a mean μ_k and covariance Σ_k . The probability of each Gaussian is denoted as $p(c_k) = \pi_k$ with $\sum_{k=1}^K \pi_k = 1$. The optimal number of clusters K is obtained, by minimizing the Bayesian Information Criterion (BIC). The BIC balances model complexity and fit quality, as described by Schwarz (1978) and in Text S3 of Supporting Information S1.

2.3. Variability Estimation

The GMM allows assigning a probability, $p(c_k | z(t))$, to each data point, $z(t)$, that quantifies its likelihood of belonging to category c_k . These are the category memberships of the data point (Text S4 in Supporting Information S1), which are inherently fuzzy and non-binary (i.e. they are probabilities between 0 and 1), and allow us to describe ENSO events in terms of their likelihood of occurrence. As a consequence, we can decompose a variable $y(t)$, for instance, SSHA, into the contributions of each category, by

$$y(t) = \sum_k p(c_k | z(t)) \cdot y(t) := \sum_k y_k(t) \quad (2)$$

where $y_k(t)$ is defined as the contribution of category c_k . Averaging $y_k(t)$ over time corresponds to a weighted average, with the weights being the categorical memberships (Text S5 in Supporting Information S1). Similarly, we can write the variance $\langle y^2 \rangle$, as

$$\langle y^2 \rangle = \left\langle \left(\sum_k y_k \right)^2 \right\rangle = \sum_k \langle y_k^2 \rangle + \sum_{l \neq m} \langle y_l y_m \rangle, \quad (3)$$

where $\langle y_k^2 \rangle$ is the variance contribution of category c_k and $\langle y_l y_m \rangle$ is the co-variability of categories l and m .

3. Results

3.1. ENSO Diversity Is Well Explained by Five Categories

The two most dominant EOFs of all eight SSTA data sets combined (Table S1 in Supporting Information S1) present the well-known spatial patterns associated with ENSO, that is, EOF1 depicts the typical ENSO pattern with anomalies in the Central-Eastern Pacific, while EOF2 exhibits an east-west dipole structure (Figure S2 in Supporting Information S1). Projection of the monthly SSTA of all boreal winter (December-January-February) El Niño and La Niña events onto EOF1 and EOF2, produces a distribution in the corresponding PC1–PC2 space with a wide, boomerang-like shape (Figure 1a; Figure S3 in Supporting Information S1). This nonlinear relationship between PC1 and PC2 has been considered an expression of key ENSO dynamics (Cai et al., 2018; Ham & Kug, 2012; Karamperidou et al., 2017; Takahashi & Dewitte, 2016), and used in the selection of models to

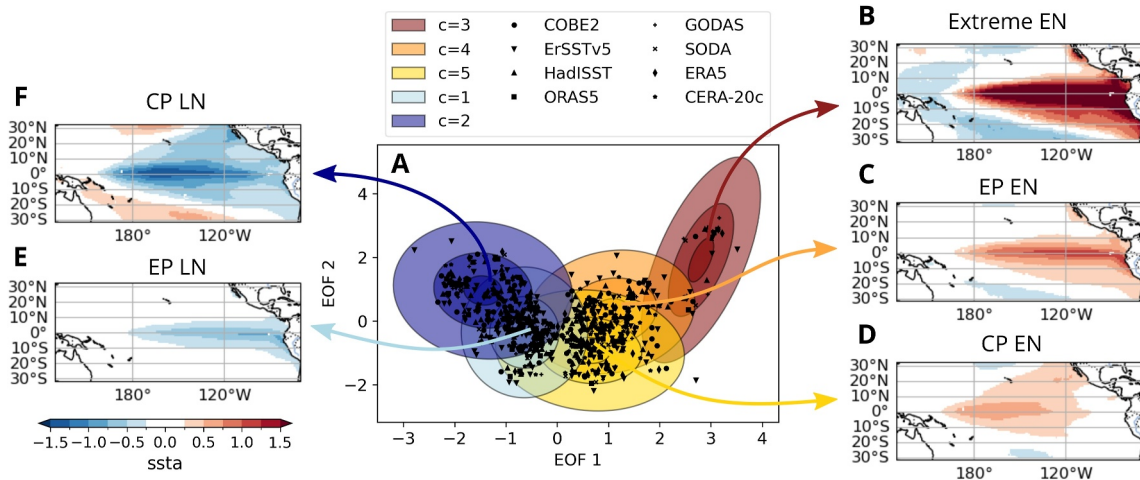


Figure 1. El Niño and La Niña categories in PC1-PC2 space. Monthly boreal winter (DJF) SSTAs of El Niño and La Niña events of all reanalysis products (see Table S1 in Supporting Information S1) projected onto the PC1-PC2 space and fitted by a Gaussian Mixture Model. Each event (DJF averages are shown as black dots in (a)) has a probability of belonging to each of the five categories (colored Gaussians in (a)). Pacific sea surface temperature anomalies composites for each category are obtained by using the category membership as weights for the averages, depicted in panels (b)–(f). We obtain three El Niño-like patterns: (b) *Extreme EN*, (c) *Strong EN*, and (d) *Weak EN*, while La Niña events form two categories: (e) *Weak LN* and (f) *Strong LN*.

consider for examining future projections (Cai et al., 2018, 2021). The nonlinear relationship itself can be accounted for by using a nonlinear transformation in place of the linear EOF-based transform, for example, an autoencoder, and in that case, the boomerang-like shape is replaced by a simple linear relation between the two latent dimensions (Figure S4 and Text S2 in Supporting Information S1).

The distribution of boreal winter El Niño and La Niña months in the PC1-PC2 space does not exhibit clear gaps visually but their density varies, suggesting a categorical structure (Takahashi & Dewitte, 2016). We model this distribution using a GMM with $k = 5$ categories (Equation 1), a number determined using the BIC to ensure parsimony (see Text S3, Figure S5a in Supporting Information S1). The five Gaussians are arranged in a row along the boomerang-shaped distribution from the coldest events at the leftmost tip to the warmest events at the rightmost end (Figure 1a).

We use the category memberships, $p(c_k|z(t))$, as weights for averaging the Pacific SSTAs of each category (Text S5 in Supporting Information S1) and find three El Niño-like patterns (Figures 1b–1d), and two La Niña-like patterns (Figures 1e and 1f). Besides the different zonal locations of maximum warming/cooling, their defining factor is the tropical Pacific SSTA intensity. Hence, we will refer to the three El Niño categories as *Extreme EN* (Figure 1b), *Strong EN* (Figure 1c) and *Weak EN* (Figure 1d), and to the La Niña categories as *Weak LN* (Figure 1e) and *Strong LN* (Figure 1f). We find that the overall clustering of the SSTA patterns into the five categories is robust (Text S6 in Supporting Information S1) upon changing the number of EOFs (Figures S5b, S6, and S7b in Supporting Information S1), incorporating SSHA data along with the SSTA (Figures S8k–S8o in Supporting Information S1), or varying the latitudinal range of the input (Figures S8f–S8j). For comparison, we show the Gaussians for $k = 4$ (Figure S9 in Supporting Information S1), and $k = 6$ (Figure S10 in Supporting Information S1) categories.

The mean category membership for each boreal winter averaged across the data sets results in five time series of probabilities—one for each category—which reflect the likelihood of their occurrences (Figure 2). We find that the indices are not sensitive to the data set used for their estimation, as seen in the relatively small spread of the membership probabilities over the data sets at each time point (Figure S11 in Supporting Information S1). As with the number of clusters, the category membership is also robust to changes in the number of variables, spatial domain, and the use of nonlinear encoding (Figure S12 in Supporting Information S1).

Comparing the category membership series for *Strong* and *Weak EN* events (Figures 2b and 2c) to two conventional classifications—the Niño3–Niño4 classification by Kug et al. (2009) and the EOF-based E/C classification by Takahashi et al. (2011)—we find that our classification mostly agrees with them (Table S2, Text S7 in Supporting Information S1). Differences, when they do occur, correspond to differences between the other

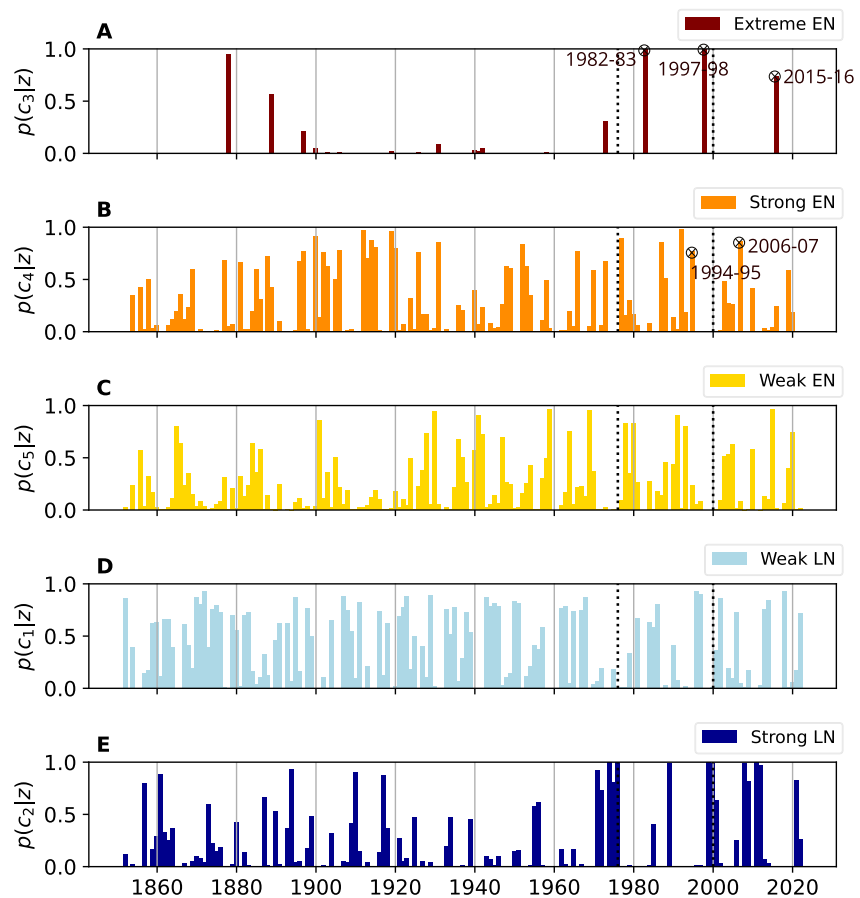


Figure 2. Probabilistic category membership. The Gaussian Mixture Model in Figure 1 allows us to estimate the likelihood, $p(c_k|z(t))$, of each El Niño and La Niña winter month, $z(t)$, to belong to each of the categories, c_k (Text S4 in Supporting Information S1). An event belongs only to one category when its probability is 1. However, many events have shared probabilities across several categories. The categories are sorted in the following order (top to bottom): (a) *Extreme EN*, (b) *Strong EN*, (c) *Weak EN*, (d) *Weak LN*, and (e) *Strong LN*. For visual reasons, we average the monthly probabilities over each winter (DJF) and over reanalysis products. The dashed lines indicate the reported shifts in ENSO variability in 1976–1977 and 2000.

classifications as well (Capotondi et al., 2015; Pascolini-Campbell et al., 2015; J.-Y. Yu & Kim, 2013). The two El Niños of 1994–1995 and 2006–2007, however, are classified by both conventional classifications as CP events, whereas we find them to be *Strong EN* events (Table S2 in Supporting Information S1). This is likely because the warm water anomalies span from the Central to the EP during the duration of these events, leading to possible ambiguities in the event definition (Figures S13c and S13h in Supporting Information S1). We also note that unlike the 1982–1983 and 1997–1998 events, which unambiguously belonged to the *Extreme EN* category, the 2015–2016 event also has a nonzero membership in the *Strong EN* category, confirming its mixed nature.

3.2. Extreme EN Events Are Different From Strong EN Events

A key distinction of our ENSO categorization from conventional methods is the identification of the extreme El Niños as a separate class. While our *Weak EN* category corresponds to the conventional CP El Niño type, the conventional EP El Niño type is split into *Extreme EN* and *Strong EN* categories (Text S7, Table S2 in Supporting Information S1). SSTA composites of conventional EP El Niño events (Figures S14a, S14c, S14e, S15b in Supporting Information S1) exhibit the maximum warming in the EP. The maximum warming is however strongly influenced by the few extreme EN events (1982–1983, 1997–1998, 2015–2016), with an eastward shift of the peak toward the CP when we exclude the extreme events (Figures S14b, S14d, and S14f in Supporting Information S1).

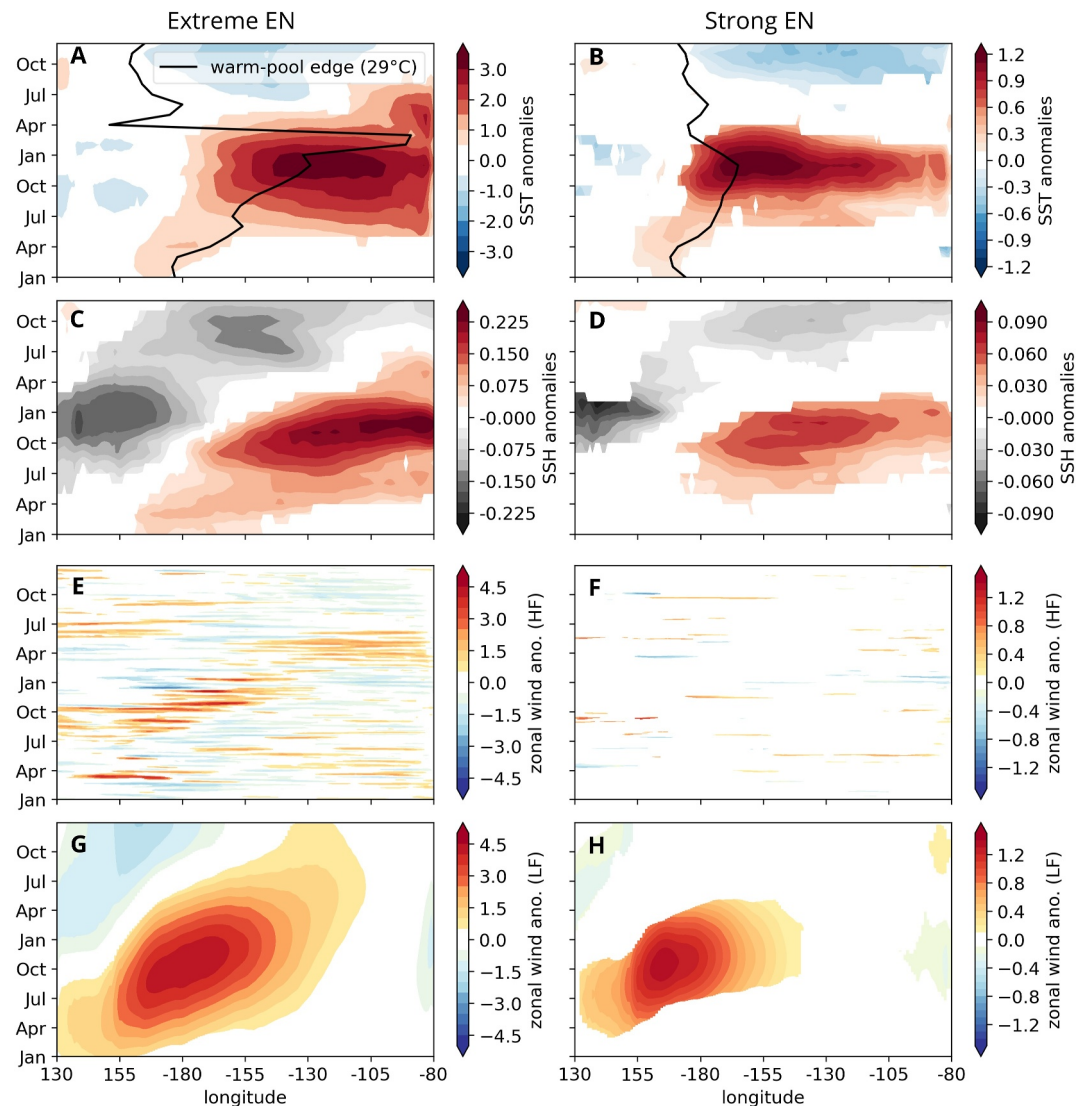


Figure 3. Extreme EN and Strong EN category. (a and b) Hovmöller diagrams of sea surface temperature anomalies (SSTA), (c and d) SSHA, (e and f) high-frequency (HF) zonal wind anomalies, and (g and h) low-frequency (LF) zonal wind anomalies are obtained by meridional averages (5°S – 5°N) of each month in the year preceding and succeeding El Niño events. Each 2-year period is weighted by the corresponding DJF average category membership probability (Figure 2). The black line in (a) and (b) indicates the warm-pool edge, that is, the 29°C SST isotherm (Text S8 in Supporting Information S1). Only values that are statistically significant above the 95th percentile are displayed (Text S9 in Supporting Information S1). SSTA and SSHA are taken from ORAS5 (1958–2022), while 10-m zonal winds, with their HF- and LF components (Text S1 in Supporting Information S1) are computed from ERA5.

The separation of *Extreme EN* from *Strong EN* events highlights differences in their impacts. We find that during *Extreme EN* events, statistically significant (at 95% confidence) warmer-than-average SSTs and negative OLR anomalies occur in the Indian Oceans (Figures S16a and S16k in Supporting Information S1), which are not significant for *Strong EN* (Figures S16b and S16l in Supporting Information S1).

The two categories also differ in their evolution, analyzed using Hovmöller diagrams for the year preceding and succeeding an event (Figure 3; Figure S17 in Supporting Information S1). *Extreme EN* events show significant warm water volume anomalies, as described by SSHA, around the dateline already in the spring before an event, corresponding with a shift of the warm pool edge near the dateline (black contour line in Figure 3a). The *Extreme EN* onset phase also shows strong positive high-frequency (HF) and low-frequency (LF) zonal wind components to the west of the dateline, during the preceding spring, extending further east as the event develops to its mature

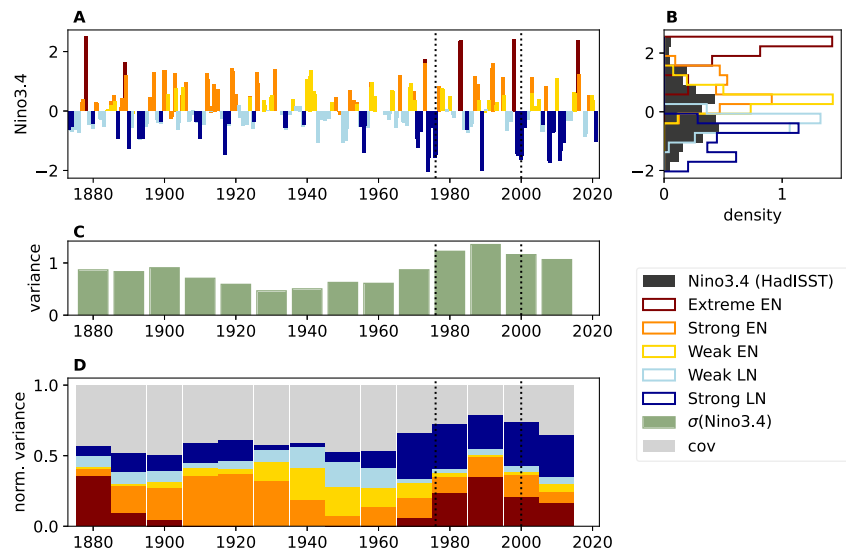


Figure 4. Low-frequency changes of El Niño Southern Oscillation (ENSO) variance. For each category, the Niño3.4 index is multiplied by their category membership probabilities (a). The histogram of Niño3.4 intensities (b), highlights different sea surface temperature anomalies amplitudes between categories. The 20-year running variance of Niño3.4 every 10 years (c), is used to normalize the 20-year running variance of each category (d). *Extreme EN* and *Strong EN* categories dominate the Niño3.4 variance in the early and late twentieth century. The variance shift in 1976–1977 and 2000 (dashed lines) highlight reported changes in ENSO variability. The Niño3.4 index is taken from HadISST (Rayner et al., 2003).

phase (Figures 3e and 3g). *Strong EN* events, on the other hand, have much weaker HF winds (Figure 3f), and a more limited eastward extension of LF winds, warm water volume, and warm pool edge (Figures 3h, 3d, and 3b).

These findings corroborate ideas presented in prior research on the impact of the Walker circulation's zonal shift (Thual & Dewitte, 2023) and the influence of stochastic high-frequency winds, called Westerly Wind Bursts, on ENSO Diversity (Capotondi et al., 2018; Fedorov et al., 2015; Puy et al., 2019).

3.3. Interdecadal ENSO Variability Is Driven by Strong and Extreme Events

The membership probabilities of each category (Figure 2) encode a distinct pattern of decadal-to-multidecadal ENSO variability. In particular, the *Strong LN* and the *Extreme EN* categories show a markedly prominent low-frequency variability, which is less evident in other categories. To quantify the low-frequency variation of ENSO, we multiply the Niño3.4 index (from HadISST) by the corresponding membership probabilities for each category (Equation 2, Figure 4a) and calculate their 20-year running variances every 10 years (Equation 3). The variance of each category is normalized by the 20-year running variance of the Niño3.4 index (Figure 4c) to determine their relative contributions.

The total variance of the Niño3.4 index shows a low-frequency modulation, with a minimum around 1920–1960, followed by an increasing trend, which is consistent with the shift in the mean and variance of ENSO after the so-called “1976–1977 climate shift” (e.g., Miller et al., 1994) (dashed line in Figure 4c). A slight decrease in variance is noticeable after the year 2000, in line with the other reported climate shift (e.g., McPhaden, 2012). While changes are noticeable in the variance of all categories, only minor contributions to the total Niño3.4 variance are observed for the *Weak LN* and *Weak EN* categories (Figure 4d). The *Strong LN* category exhibits a substantial contribution starting around 1970, and the *Strong EN* category dominates the variance from 1890 to ~1930. Meanwhile, the contribution of the *Extreme EN* category is particularly visible toward the end of the nineteenth century and after 1980. These results are robust against variations in window size (Figure S18 in Supporting Information S1) and using different reanalysis products (Figure S19 in Supporting Information S1).

Between 20% and 40% of the decadal variance is due to the covariance between the different ENSO categories (denoted as *cov* in Figure 4d). The covariance captures mainly the contribution of co-occurrences of different categories to the overall variance in a decade. However, other factors such as events with intermediate values of category memberships and statistical errors in estimating the GMM categories also influence the covariance. Our

statistical approach does not allow us to assess the dynamical underpinning of these decadal changes in the contribution of the different ENSO categories. ENSO decadal modulation is often associated with changes in the mean state, but it is not clear whether mean state changes are induced by influences from the extratropical Pacific or other ocean basins, or result as a residual of random variations of ENSO itself (Capotondi et al., 2023). Some studies, however, suggest that some ENSO events could induce decadal phase transitions through either nonlinear dynamical heating (Liu et al., 2022) or by inducing a discharge of upper ocean heat content in the off-equatorial Western Pacific (Meehl et al., 2021).

Our results provide novel insights into low-frequency changes in ENSO variance, which combines changes in frequency and intensity. We find that although the magnitude of total variance contributed by EP warming events (i.e., *Extreme EN* and *Strong EN* events combined) since the turn of the twentieth century is comparable to that seen during the period from the 1880s–1940s, the variance in the recent decades has been dominated by the *Extreme EN* category, a result consistent with the statistically significant change in ENSO properties in the late 1970s (Capotondi & Sardeshmukh, 2017). This shift was associated with a weakening of the easterly trade winds and a zonal reduction of the equatorial thermocline slope, conditions favoring stronger El Niño events. Linked to the increased contributions from *Extreme EN* events is the concurrent increase in the contributions of *Strong LNs* since the 1970s (dark blue in Figure 4d), manifested in very strong, multi-year events starting around 1970 (Figure 4a). These results are consistent with a higher likelihood of stronger CP La Niñas following the heat discharge of strong El Niños, as exemplified by the 1998–1999 La Niña event after the extreme 1997–1998 El Niño (Cai et al., 2015; Geng et al., 2023). While the increasing contribution of *Extreme EN* and *Strong LN* to ENSO variance starting around 1970 aligns with results from climate model simulations (Cai et al., 2021; Gan et al., 2023), our findings more specifically highlight the key role played by *Strong LN* in the ENSO variance changes after 1970.

We also find that during the “quiescent” period of ENSO, roughly from the 1930s to the 1960s, most of the ENSO variability originated from CP warming and EP cooling events, that is, from the weaker event types, while the influence of CP warming on the ENSO variance in recent decades has been almost negligible. This latter result is in apparent disagreement with the reported increase in intensity and frequency of CP events since 1980 (Lee & McPhaden, 2010), and especially after 2000 (dashed line in Figure 4d; (McPhaden et al., 2011)). The discrepancy may be related to the multi-decadal windows used to examine the ENSO variance (Figure 4d and Figure S18 in Supporting Information S1), which may emphasize the contribution of extreme El Niño relative to that of weaker CP events. The inclusion in our analysis of the 2015–2016 El Niño event, which was missing in the records considered by the earlier studies, may have further enhanced the contribution of the most intense events.

4. Discussion

We present a new approach for studying the influence of ENSO diversity on low-frequency changes in ENSO variance. In particular, we use a GMM within the low-dimensional PC1-PC2 space of monthly SSTA, which enables the assignment of non-binary event category memberships. We identify two La Niña categories (*Weak LN*, *Strong LN*) and three El Niño categories (*Extreme EN*, *Strong EN*, *Weak EN*), which combine the two dimensions of ENSO diversity—longitudinal location of maximum SSTA and its intensity. A key contribution of our work involves utilizing the membership probabilities to determine how each of the five categories individually affects the overall decadal variability in the Niño3.4 region. We find that the increasing frequency of both *Extreme EN* and *Strong LN* are the primary drivers of the increased ENSO variance post-1970. While these findings are consistent with previous studies that also detected an increase in extreme ENSO events in the second half of the twentieth century (Cai et al., 2018, 2023), our results further highlight the key role played by the increasing frequency of *Strong LN* in these ENSO variance changes.

The proposed fuzzy clustering approach could also be used to quantify how well climate models represent ENSO diversity, akin to Dieppois et al. (2021) and Ayar et al. (2023). A preliminary analysis of the Community Earth System Model version 2 (CESM2) shows that this model only exhibits four ENSO categories instead of five (Text S10, Figure S20 in Supporting Information S1), a discrepancy which cannot be explained by the different number of samples or other technical choices. Specifically, the *Extreme EN* category is missing in the model. While ENSO in CESM2 has an amplitude larger than observed, modeled SSTAs tend to occur preferentially in the central equatorial Pacific, with a more limited range of ENSO spatial patterns (Capotondi, Deser, et al., 2020), a behavior that seems to align with the model's inability to simulate extreme events in the EP. In addition, the model

appears to underestimate ENSO's nonlinearities, as quantified by the quadratic fit coefficient, α , in PC1-PC2 space (Cai et al., 2018; Dommenget et al., 2013; Karamperidou et al., 2017), which is smaller in CESM2 compared to reanalysis (Figure S21 in Supporting Information S1). Although CESM2 exhibits a pattern of SST decadal variability that is relatively similar to the observed (Capotondi, Deser, et al., 2020), the amplitude of the decadal ENSO modulation appears underestimated in the model (Figure S22 in Supporting Information S1) relative to observations (Figure 4). In the absence of the Extreme El Niño category in the model, most of the decadal variations are associated with the occurrence of Strong El Niño and, to a lesser degree, strong La Niña events. These results suggest the possibility that the model's inability to represent the full range of ENSO diversity could also hinder its ability to realistically simulate the low-frequency modulation of ENSO variance, a possibility that warrants further future investigations across multi-model ensembles. An extensive examination of several climate models using our methodology is beyond the scope of this paper. However, our analysis of CESM2 demonstrates the potential value of our approach for achieving a detailed assessment of ENSO diversity in climate models. Such an investigation, as well as the analysis of possible changes in ENSO types in future climate scenarios, will be considered in subsequent studies.

Data Availability Statement

The data on which this article is based are publicly available in H.-M. Zhang et al. (2019), Hersbach et al. (2020), Ishii et al. (2005), Rayner et al. (2003), Copernicus Climate Change Service (2021), Giese and Ray (2011), Behringer et al. (1998), and Laloyaux et al. (2018), with their details are listed in Table S1 of Supporting Information S1. Our code is publicly available under Schlör (2023) and <https://github.com/jakob-schloer/LatentGMM.git>.

Acknowledgments

The authors thank the International Max Planck Research School for Intelligent Systems (IMPRS-IS) for supporting J. Schlör and F. Strnad. Furthermore, we express our gratitude to the NOAA Physical Science Laboratory for making their resources available for this study. Funded by the Deutsche Forschungsgemeinschaft (DFG, German Research Foundation) under Germany's Excellence Strategy—EXC number 2064/1—Project number 390727645. We acknowledge support from the Open Access Publication Fund of the University of Tübingen. A. Capotondi was supported by the NOAA Climate Program Office's Climate Variability and Predictability (CVP) and Modeling, Analysis, Predictions and Projections (MAPP) programs and by DOE Award No. DE-SC0023228. Open Access funding enabled and organized by Projekt DEAL.

References

- Abdelkader Di Carlo, I., Braconnot, P., Carré, M., Elliot, M., & Marti, O. (2023). Different methods in assessing El Niño flavors lead to opposite results. *Geophysical Research Letters*, 50(15), e2023GL104558. <https://doi.org/10.1029/2023GL104558>
- Ashok, K., Behera, S. K., Rao, S. A., Weng, H., & Yamagata, T. (2007). El Niño Modoki and its possible teleconnection. *Journal of Geophysical Research*, 112(11), C11007. <https://doi.org/10.1029/2006JC003798>
- Ayar, P. V., Battisti, D. S., Li, C., King, M., Vrac, M., & Tjiputra, J. (2023). A regime view of ENSO flavors through clustering in CMIP6 models. *Earth's Future*, 11(11), e2022EF003460. <https://doi.org/10.1029/2022EF003460>
- Behringer, D. W., Ji, M., & Leetmaa, A. (1998). An improved coupled model for ENSO prediction and implications for ocean initialization. Part I: The ocean data assimilation system. *Monthly Weather Review*, 126(4), 1013–1021. [https://doi.org/10.1175/1520-0493\(1998\)126<1013:AIICMFE>2.0.CO;2](https://doi.org/10.1175/1520-0493(1998)126<1013:AIICMFE>2.0.CO;2)
- Beniche, M., Vialard, J., Lengaigne, M., Voldoire, A., Srinivas, G., & Hall, N. M. J. (2024). A distinct and reproducible teleconnection pattern over North America during extreme El Niño events. *Scientific Reports*, 14(1), 2457. <https://doi.org/10.1038/s41598-024-52580-9>
- Cai, W., Ng, B., Geng, T., Jia, F., Wu, L., Wang, G., et al. (2023). Anthropogenic impacts on twentieth-century ENSO variability changes. *Nature Reviews Earth & Environment*, 4(6), 407–418. <https://doi.org/10.1038/s43017-023-00427-8>
- Cai, W., Santoso, A., Collins, M., Dewitte, B., Karamperidou, C., Kug, J.-S., et al. (2021). Changing El Niño–Southern Oscillation in a warming climate. *Nature Reviews Earth & Environment*, 2(9), 628–644. <https://doi.org/10.1038/s43017-021-00199-z>
- Cai, W., Wang, G., Dewitte, B., Wu, L., Santoso, A., Takahashi, K., et al. (2018). Increased variability of eastern Pacific El Niño under greenhouse warming. *Nature*, 564(7735), 201–206. <https://doi.org/10.1038/s41586-018-0776-9>
- Cai, W., Wang, G., Santoso, A., McPhaden, M. J., Wu, L., Jin, F.-F., et al. (2015). Increased frequency of extreme La Niña events under greenhouse warming. *Nature Climate Change*, 5(2), 132–137. <https://doi.org/10.1038/nclimate2492>
- Capotondi, A. (2013). ENSO diversity in the NCAR CCSM4 climate model. *Journal of Geophysical Research: Oceans*, 118(10), 4755–4770. <https://doi.org/10.1002/jgrc.20335>
- Capotondi, A., Deser, C., Phillips, A. S., Okumura, Y., & Larson, S. M. (2020). ENSO and Pacific decadal variability in the Community Earth System Model version 2. *Journal of Advances in Modeling Earth Systems*, 12(12), e2019MS002022. <https://doi.org/10.1029/2019MS002022>
- Capotondi, A., McGregor, S., McPhaden, M. J., Cravatte, S., Holbrook, N. J., Imada, Y., et al. (2023). Mechanisms of tropical Pacific decadal variability. *Nature Reviews Earth & Environment*, 4(11), 754–769. <https://doi.org/10.1038/s43017-023-00486-x>
- Capotondi, A., & Sardeshmukh, P. D. (2017). Is El Niño really changing? *Geophysical Research Letters*, 44(16), 8548–8556. <https://doi.org/10.1002/2017GL074515>
- Capotondi, A., Sardeshmukh, P. D., & Ricciardulli, L. (2018). The nature of the stochastic wind forcing of ENSO. *Journal of Climate*, 31(19), 8081–8099. <https://doi.org/10.1175/JCLI-D-17-0842.1>
- Capotondi, A., Wittenberg, A. T., Newman, M., Lorenzo, E. D., Yu, J. Y., Braconnot, P., et al. (2015). Understanding ENSO diversity. *Bulletin of the American Meteorological Society*, 96(6), 921–938. <https://doi.org/10.1175/BAMS-D-13-00117.1>
- Copernicus Climate Change Service. (2021). ORAS5 global ocean reanalysis monthly data from 1958 to present [Dataset]. *Copernicus Climate Change Service (C3S) Climate Data Store (CDS)*. <https://doi.org/10.24381/CDS.67E8EEB7>
- Dieppois, B., Capotondi, A., Pohl, B., Chun, K. P., Monerie, P.-A., & Eden, J. (2021). ENSO diversity shows robust decadal variations that must be captured for accurate future projections. *Communications Earth & Environment*, 2(1), 212. <https://doi.org/10.1038/s43247-021-00285-6>
- Dommenget, D., Bayr, T., & Frauen, C. (2013). Analysis of the non-linearity in the pattern and time evolution of El Niño southern oscillation. *Climate Dynamics*, 40(11), 2825–2847. <https://doi.org/10.1007/s00382-012-1475-0>
- Fedorov, A. V., Hu, S., Lengaigne, M., & Guilyardi, E. (2015). The impact of westerly wind bursts and ocean initial state on the development, and diversity of El Niño events. *Climate Dynamics*, 44(5), 1381–1401. <https://doi.org/10.1007/s00382-014-2126-4>

- Gan, R., Liu, Q., Huang, G., Hu, K., & Li, X. (2023). Greenhouse warming and internal variability increase extreme and central Pacific El Niño frequency since 1980. *Nature Communications*, 14(1), 394. <https://doi.org/10.1038/s41467-023-36053-7>
- Geng, T., Jia, F., Cai, W., Wu, L., Gan, B., Jing, Z., et al. (2023). Increased occurrences of consecutive La Niña events under global warming. *Nature*, 619(7971), 774–781. <https://doi.org/10.1038/s41586-023-06236-9>
- Giese, B. S., & Ray, S. (2011). El Niño variability in simple ocean data assimilation (SODA), 1871–2008. *Journal of Geophysical Research*, 116(2), C02024. <https://doi.org/10.1029/2010JC006695>
- Grothe, P. R., Cobb, K. M., Liguori, G., Di Lorenzo, E., Capotondi, A., Lu, Y., et al. (2020). Enhanced El Niño–Southern oscillation variability in recent decades. *Geophysical Research Letters*, 47(7), e2019GL083906. <https://doi.org/10.1029/2019GL083906>
- Ham, Y.-G., & Kug, J.-S. (2012). How well do current climate models simulate two types of El Niño? *Climate Dynamics*, 39(1–2), 383–398. <https://doi.org/10.1007/s00382-011-1157-3>
- Hersbach, H., Bell, B., Berrisford, P., Hirahara, S., Nicolas, J., Peubey, C., et al. (2020). The ERA5 global reanalysis. *Quarterly Journal of the Royal Meteorological Society*, 146(730), 1999–2049. <https://doi.org/10.1002/qj.3803>
- Ishii, M., Shouji, A., Sugimoto, S., & Matsumoto, T. (2005). Objective analyses of sea-surface temperature and marine meteorological variables for the 20th century using ICOADS and the Kobe Collection. *International Journal of Climatology*, 25(7), 865–879. <https://doi.org/10.1002/joc.1169>
- Kao, H. Y., & Yu, J. Y. (2009). Contrasting eastern-Pacific and central-Pacific types of ENSO. *Journal of Climate*, 22(3), 615–632. <https://doi.org/10.1175/2008JCLI2309.1>
- Karamperidou, C., Jin, F.-F., & Conroy, J. L. (2017). The importance of ENSO nonlinearities in tropical Pacific response to external forcing. *Climate Dynamics*, 49(7), 2695–2704. <https://doi.org/10.1007/s00382-016-3475-y>
- Kug, J. S., Jin, F. F., & An, S. I. (2009). Two types of El Niño events: Cold tongue El Niño and warm pool El Niño. *Journal of Climate*, 22(6), 1499–1515. <https://doi.org/10.1175/2008JCLI2624.1>
- Lalouay, P., de Boisseson, E., Balmaseda, M., Bidlot, J.-R., Broennimann, S., Buizza, R., et al. (2018). CERA-20C: A coupled reanalysis of the twentieth century. *Journal of Advances in Modeling Earth Systems*, 10(5), 1172–1195. <https://doi.org/10.1029/2018MS001273>
- Larkin, N. K., & Harrison, D. E. (2005). Global seasonal temperature and precipitation anomalies during El Niño autumn and winter. *Geophysical Research Letters*, 32(16), L16705. <https://doi.org/10.1029/2005GL022860>
- Lawman, A. E., Di Nezio, P. N., Partin, J. W., Dee, S. G., Thirumalai, K., & Quinn, T. M. (2022). Unraveling forced responses of extreme El Niño variability over the Holocene. *Science Advances*, 8(9), eabm4313. <https://doi.org/10.1126/sciadv.abm4313>
- Lee, T., & McPhaden, M. J. (2010). Increasing intensity of El Niño in the central-equatorial Pacific. *Geophysical Research Letters*, 37(14), L14603. <https://doi.org/10.1029/2010GL044007>
- Liu, C., Zhang, W., Jin, F.-F., Stuecker, M. F., & Geng, L. (2022). Equatorial origin of the observed tropical Pacific quasi-decadal variability from ENSO nonlinearity. *Geophysical Research Letters*, 49(10), e2022GL097903. <https://doi.org/10.1029/2022GL097903>
- Lou, J., Newman, M., & Hoell, A. (2023). Multi-decadal variation of ENSO forecast skill since the late 1800s. *npj Climate and Atmospheric Science*, 6(1), 1–14. <https://doi.org/10.1038/s41612-023-00417-z>
- McPhaden, M. J. (2004). Evolution of the 2002/03 El Niño. *Bulletin of the American Meteorological Society*, 85(5), 677–696. <https://doi.org/10.1175/BAMS-85-5-677>
- McPhaden, M. J. (2012). A 21st century shift in the relationship between ENSO SST and warm water volume anomalies. *Geophysical Research Letters*, 39(9), L09706. <https://doi.org/10.1029/2012GL051826>
- McPhaden, M. J., Lee, T., & McClurg, D. (2011). El Niño and its relationship to changing background conditions in the tropical Pacific Ocean. *Geophysical Research Letters*, 38(15), L15709. <https://doi.org/10.1029/2011GL048275>
- Meehl, G. A., Teng, H., Capotondi, A., & Hu, A. (2021). The role of interannual ENSO events in decadal timescale transitions of the Interdecadal Pacific Oscillation. *Climate Dynamics*, 57(7), 1933–1951. <https://doi.org/10.1007/s00382-021-05784-y>
- Miller, A. J., Cayan, D. R., Barnett, T. P., Graham, N. E., & Oberhuber, J. M. (1994). The 1976–77 climate shift of the Pacific Ocean. *Oceanography*, 7(1), 21–26. <https://doi.org/10.5670/oceanog.1994.11>
- Paek, H., Yu, J.-Y., & Qian, C. (2017). Why were the 2015/2016 and 1997/1998 extreme El Niños different? *Geophysical Research Letters*, 44(4), 1848–1856. <https://doi.org/10.1002/2016GL071515>
- Parsons, L., Haque, E., & Liu, H. (2004). Subspace clustering for high dimensional data: A review. *SIGKDD Explorations Newsletter*, 6(1), 90–105. <https://doi.org/10.1145/1007730.1007731>
- Pascolini-Campbell, M., Zanchettin, D., Bothe, O., Timmreck, C., Matei, D., Jungclauss, J. H., & Graf, H. F. (2015). Toward a record of Central Pacific El Niño events since 1880. *Theoretical and Applied Climatology*, 119(1–2), 379–389. <https://doi.org/10.1007/s00704-014-1114-2>
- Puy, M., Vialard, J., Lengaigne, M., Guilyardi, E., DiNezio, P. N., Voldoire, A., et al. (2019). Influence of westerly wind events stochasticity on El Niño amplitude: The case of 2014 vs. 2015. *Climate Dynamics*, 52(12), 7435–7454. <https://doi.org/10.1007/s00382-017-3938-9>
- Rayner, N. A., Parker, D. E., Horton, E. B., Folland, C. K., Alexander, L. V., Rowell, D. P., et al. (2003). Global analyses of sea surface temperature, sea ice, and night marine air temperature since the late nineteenth century. *Journal of Geophysical Research*, 108(D14), 4407. <https://doi.org/10.1029/2002JD002670>
- Rodrigues, R. R., Haarsma, R. J., Campos, E. J. D., & Ambrizzi, T. (2011). The impacts of inter-El Niño variability on the tropical Atlantic and northeast Brazil climate. *Journal of Climate*, 24(13), 3402–3422. <https://doi.org/10.1175/2011JCLI3983.1>
- Santoso, A., McPhaden, M. J., & Cai, W. (2017). The defining characteristics of ENSO extremes and the strong 2015/2016 El Niño. *Reviews of Geophysics*, 55(4), 1079–1129. <https://doi.org/10.1002/2017RG000560>
- Schlör, J. (2023). Jakob-schloer/LatentGMM: Revisions #1 (v2.0) [Software]. *Zenodo*. <https://doi.org/10.5281/zenodo.10144391>
- Schwarz, G. (1978). Estimating the dimension of a model. *Annals of Statistics*, 6(2), 461–464. <https://doi.org/10.1214/aos/1176344136>
- Shin, N.-Y., Kug, J.-S., McCormack, F. S., & Holbrook, N. J. (2021). The double-peaked El Niño and its physical processes. *Journal of Climate*, 34(4), 1291–1303. <https://doi.org/10.1175/JCLI-D-20-0402.1>
- Strnad, F. M., Schlör, J., Fröhlich, C., & Goswami, B. (2022). Teleconnection patterns of different El Niño types revealed by climate network curvature. *Geophysical Research Letters*, 49(17), e2022GL098571. <https://doi.org/10.1029/2022GL098571>
- Takahashi, K., & Dewitte, B. (2016). Strong and moderate nonlinear El Niño regimes. *Climate Dynamics*, 46(5–6), 1627–1645. <https://doi.org/10.1007/s00382-015-2665-3>
- Takahashi, K., Montecinos, A., Goubanova, K., & Dewitte, B. (2011). ENSO regimes: Reinterpreting the canonical and Modoki El Niño. *Geophysical Research Letters*, 38(10), L10704. <https://doi.org/10.1029/2011GL047364>
- Thual, S., & Dewitte, B. (2023). ENSO complexity controlled by zonal shifts in the Walker circulation. *Nature Geoscience*, 16(4), 328–332. <https://doi.org/10.1038/s41561-023-01154-x>
- Wang, G., & Hendon, H. H. (2007). Sensitivity of Australian rainfall to inter-El Niño variations. *Journal of Climate*, 20(16), 4211–4226. <https://doi.org/10.1175/JCLI4228.1>

- Yu, J.-Y., & Kim, S. T. (2013). Identifying the types of major El Niño events since 1870. *International Journal of Climatology*, 33(8), 2105–2112. <https://doi.org/10.1002/joc.3575>
- Zhang, H.-M., Huang, B., Lawrimore, J. H., Menne, M. J., & Smith, T. M. (2019). NOAA Global Surface Temperature Dataset (NOAA GlobalTemp), Version 5.0 [Dataset]. *NOAA National Centers for Environmental Information*. <https://doi.org/10.25921/9qth-2p70>

References From the Supporting Information

- Bishop, C. M. (2006). *Pattern recognition and machine learning*. Springer.
- Cai, W., Wu, L., Lengaigne, M., Li, T., McGregor, S., Kug, J.-S., et al. (2019). Pantropical climate interactions. *Science*, 363(6430), eaav4236. <https://doi.org/10.1126/science.aav4236>
- Capotondi, A., Wittenberg, A. T., Kug, J.-S., Takahashi, K., & McPhaden, M. J. (2020). ENSO diversity. In *El Niño Southern Oscillation in a Changing Climate* (pp. 65–86). American Geophysical Union (AGU). <https://doi.org/10.1002/9781119548164.ch4>
- Chiang, J. C. H., & Vimont, D. J. (2004). Analogous Pacific and Atlantic meridional modes of tropical atmosphere–ocean variability. *Journal of Climate*, 17(21), 4143–4158. <https://doi.org/10.1175/JCLI4953.1>
- Hameed, S. N., Jin, D., & Thilakan, V. (2018). A model for super El Niños. *Nature Communications*, 9(1), 2528. <https://doi.org/10.1038/s41467-018-04803-7>
- Holm, S. (1979). A simple sequentially rejective multiple test procedure. *Scandinavian Journal of Statistics*, 6(2), 65–70.
- Jiang, Z., Zheng, Y., Tan, H., Tang, B., & Zhou, H. (2017). Variational deep embedding: An unsupervised and generative approach to clustering.
- Murphy, K. P. (2013). *Machine learning: A probabilistic perspective*. MIT Press.
- Sidak, Z. (1967). Rectangular confidence regions for the means of multivariate normal distributions. *Journal of the American Statistical Association*, 62(318), 626–633. <https://doi.org/10.2307/2283989>
- Thual, S., Majda, A. J., Chen, N., & Stechmann, S. N. (2016). Simple stochastic model for El Niño with westerly wind bursts. *Proceedings of the National Academy of Sciences*, 113(37), 10245–10250. <https://doi.org/10.1073/pnas.1612002113>
- Wei, H.-H., Subramanian, A. C., Karanaskas, K. B., DeMott, C. A., Mazloff, M. R., & Balmaseda, M. A. (2021). Tropical Pacific air-sea interaction processes and biases in CESM2 and their relation to El Niño development. *Journal of Geophysical Research: Oceans*, 126(6), e2020JC016967. <https://doi.org/10.1029/2020JC016967>
- Wilks, D. S. (2019). *Statistical methods in the atmospheric sciences* (4th ed.). Elsevier.
- Wittenberg, A. T. (2009). Are historical records sufficient to constrain ENSO simulations? *Geophysical Research Letters*, 36(12), L12702. <https://doi.org/10.1029/2009GL038710>
- Yang, Q., Majda, A. J., & Chen, N. (2021). ENSO diversity in a tropical stochastic skeleton model for the MJO, El Niño, and dynamic Walker circulation. *Journal of Climate*, 34(9), 3481–3501. <https://doi.org/10.1175/JCLI-D-20-0447.1>
- Yu, G., Sapiro, G., & Mallat, S. (2010). Solving inverse problems with piecewise linear estimators: From Gaussian mixture models to structured sparsity. *arXiv*. <https://doi.org/10.48550/arXiv.1006.3056>
- Zhang, H., Clement, A., & Nezio, P. D. (2014). The South Pacific meridional mode: A mechanism for ENSO-like variability. *Journal of Climate*, 27(2), 769–783. <https://doi.org/10.1175/JCLI-D-13-00082.1>